IEEE Access
Multidisciplinary | Rapid Review | Open Access Journal

Received 4 December 2023, accepted 25 December 2023, date of publication 29 December 2023,
date of current version 5 January 2024.

Digital Object Identifier 10.1109/ACCESS.2023.3348240

RESEARCH ARTICLE

Spline-Shaped Microstrip Edge-Fed Antenna for 77 GHz Automotive Radar Systems

MARCO SALUCCI[1], (Senior Member, IEEE), LORENZO POLI[1], (Senior Member, IEEE), PAOLO ROCCA[1,2], (Fellow, IEEE), CLAUDIO MASSAGRANDE[3], (Member, IEEE), PIETRO ROSATTI[1], MOHAMMAD ABDUL HANNAN[1,4], MIRKO FACCHINELLI[1], AND ANDREA MASSA[1,5,6,7], (Fellow, IEEE)

[1]ELEDIA Research Center (ELEDIA@UniTN-University of Trento), DICAM-Department of Civil, Environmental, and Mechanical Engineering, 38123 Trento, Italy
[2]ELEDIA Research Center (ELEDIA@XIDIAN-Xidian University), Xi'an, Shaanxi 710071, China
[3]Huawei Technologies Italia, Palazzo Verrocchio, 20054 Segrate, Italy
[4]ELEDIA Research Center (ELEDIA@UniCT-University of Catania), Department of Electrical, Electronic, and Computer Engineering, 95123 Catania, Italy
[5]ELEDIA Research Center (ELEDIA@UESTC-UESTC), School of Electronic Science and Engineering, University of Electronic Science and Technology of China, Chengdu 611731, China
[6]ELEDIA Research Center (ELEDIA@TSINGHUA-Tsinghua University), Haidian, Beijing 100084, China
[7]School of Electrical Engineering, Tel Aviv University, Tel Aviv 69978, Israel

Corresponding author: Andrea Massa (andrea.massa@unitn.it)

This work benefited from the networking activities carried out within the Project "ICSC National Centre for HPC, Big Data and Quantum Computing (CN HPC)" funded by the European Union-NextGenerationEU within the PNRR Program (CUP: E63C22000970007), the Project "INSIDE-NEXT-Indoor Smart Illuminator for Device Energization and Next-Generation Communications" funded by the Italian Ministry for Universities and Research within the PRIN 2022 Program (CUP: E53D23000990001), the Project "AURORA - Smart Materials for Ubiquitous Energy Harvesting, Storage, and Delivery in Next Generation Sustainable Environments" funded by the Italian Ministry for Universities and Research within the PRIN-PNRR 2022 Program, the Project "SPEED" (Grant No. 6721001) funded by National Science Foundation of China under the Chang-Jiang Visiting Professorship Program, and the Project DICAM-EXC (Grant L232/2016) funded by the Italian Ministry of Education, Universities and Research (MUR) within the "Departments of Excellence 2023-2027" Program (CUP: E63C22003880001). The work of M. A. Hannan has been supported by the European Union under the Italian National Recovery and Resilience Plan (NRRP) of NextGenerationEU, partnership on "Telecommunications of the Future", PE0000001-program "RESTART", Structural Project "ISaCAGE".

ABSTRACT An innovative millimeter-wave (*mm*-wave) microstrip edge-fed antenna (*EFA*) for 77 GHz automotive radars is proposed. The radiator is designed under the main requirements of having (*i*) an horizontally-polarized pattern and (*ii*) a single-layer layout. Its contour is modeled with a sinusoidal spline-shaped (*SS*) profile characterized by a reduced number of geometrical descriptors, but still able to guarantee, thanks to a continuously non-uniform width, a high flexibility in the modeling for fulfilling challenging user-defined requirements. The *SS-EFA* descriptors are effectively and efficiently optimized with a customized implementation of the System-by-Design (*SbD*) paradigm. The synthesized *EFA* layout, integrated within a linear arrangement of identical replicas to account for the integration into the real radar system, exhibits suitable impedance matching, isolation, polarization purity, and stability of the beam shaping/pointing within the target band $f_{\min} = 76$ [GHz] $\leq f \leq f_{\max} = 78$ [GHz]. The experimental assessment, carried out with a Compact Antenna Test Range (*CATR*) system on a printed circuit board (*PCB*)-manufactured prototype, assesses the reliability of the outcomes from the full-wave (*FW*) simulations as well as the suitability of the synthesized *SS-EFA* for automotive radars.

INDEX TERMS Automotive radar, mm-waves, 77 [GHz] bandwidth, antenna design, spline, system-by-design (SbD).

The associate editor coordinating the review of this manuscript and approving it for publication was Tutku Karacolak.

NOMENCLATURE

ACC	Adaptive Cruise Control.
AUT	Antenna Under Test.

BDD	Beam Direction Deviation.
CATR	Compact Antenna Test Range.
CFA	Center-Fed Antenna.
DoA	Direction of Arrival.
DoF	Degree-of-Freedom.
DT	Digital Twin.
EFA	Edge-Fed Antenna.
FBW	Fractional Bandwidth.
FF	Far-Field.
FMCW	Frequency Modulated Continuous Wave.
FW	Full-Wave.
LBE	Learning-by-Examples.
LHS	Latin Hypercube Sampling.
MC	Mutual Coupling.
MIMO	Multiple-Input Multiple-Output.
OK	Ordinary Kriging.
PCB	Printed Circuit Board.
PR	Polarization Ratio.
PSO	Particle Swarm Optimizer.
RS	Resonant.
SbD	System-by-Design.
SS	Spline-Shaped.
SSE	Solution Space Exploration.
SW	Standing Wave.
TW	Travelling-Wave.

I. INTRODUCTION

Millimiter-wave (*mm*-wave) radars play an important role in many modern automotive applications ranging from active safety driver assistance systems to autonomous driving vehicles [1], [2], [3]. Thanks to the capability to measure the distance, the speed, and the direction of arrival (*DoA*) of multiple targets with low delays, they are frequently used for blind-spot detection, collision avoidance, and emergency brake assistance [4], [5]. Moreover, automotive radars are a key technology for implementing active comfort systems featuring a high robustness against environmental conditions including high temperature, darkness, and bad weather. For instance, let us consider adaptive cruise control (*ACC*) systems that allow the vehicle to autonomously accelerate or brake or stop in case of traffic jam to relieve the driver of monotonous tasks.

In order to continuously sense and monitor the surrounding environment [1], multiple receive and transmit antennas/channels are used to implement frequency modulated continuous wave (*FMCW*) multiple-input multiple-output (*MIMO*) radars and 77 [GHz] solutions are particularly attractive because of the many advantages over systems operating at lower frequencies (e.g., 24 [GHz] band [1], [6], [7]). As a matter of fact, the exploitation of the 77 [GHz] band allows one to design smaller antennas with lower volume- and weight-related costs as well as to reach a higher spatial resolution (thanks to the larger absolute bandwidth of the antenna system) and more precise *DoA* estimations [1].

As for the antenna implementation, different technological solutions have been explored in the last few years including Franklin antennas [6], series-fed microstrip arrays [8], [9], comb-line arrays [10], [11], [12], [13], lens antennas [14], dielectric resonator antennas [15], planar grid arrays [16], [17], leaky-wave antennas [18], ceramic-filled cavity resonators [19], patch arrays [20], [21], and substrate integrated wave-guides (*SIW*s) [22], [23], [24], [25], [26]. Series-fed architectures are nowadays a mainstream choice because of the limited cost, the low profile, the light weight, and the simple manufacturing/integration in automotive systems. However, the feeding mechanism is more complex than that of traditional corporate feeding networks since all the (series-connected) radiating points must be excited in-phase to afford a well-shaped broadside radiation pattern. To address such an issue, both center-fed (*CFA*s) [27], [28] and edge-fed (*EFA*s) [8] antennas have been studied. The former mitigate the beam tilting (or squint) due to the change of the electrical lengths between consecutive radiating locations at different frequencies within the working band, but they may be unsuitable for a compact integration/connection to the driving pins of a *FMCW* radar micro-chip. Otherwise, *EFA*s can be more easily closely-packed in linear array arrangements by means of simpler routing connections [8]. However, the design of *EFA*s, which can be in turn implemented both as resonant (*RS*) and travelling-wave (*TW*) structures depending on the absence or presence of a matched load placed at the termination edge on the opposite of the feeding point [29], turns out to be more challenging because of the more difficult control of each excitation phase from a single feeding point located on one edge. Generally speaking, while *TW-EFA*s usually enable a more flexible beam shaping of the far-field (*FF*) pattern, they are also characterized by a larger beam direction deviation (*BDD*) with frequency and a lower radiation efficiency because of the energy dissipated in the terminating load [29].

Concerning the polarization, several designs radiating a vertically-polarized *FF* pattern have been reported in the recent scientific literature [6], [8], [16], [29]. However, many automotive applications (including the one considered here) require an horizontal polarization because of the lower backscattering from road pavements, resulting in a reduced amount of clutter and thus allowing a more robust target detection [7], [10], [22], [23], [30], [31], [32].

Finally, another challenging requirement addressed in this work is the need for a single-layer layout. As a matter of fact, having a manufacturing process where both the radiating elements and the routing connections from/towards the controlling radar chipset can be simultaneously etched on the same face of a single dielectric substrate is highly desirable in terms of fabrication simplicity/costs and mechanical robustness to vibrations [6], [13], [16], [20]. Therefore, although providing remarkable radiation/bandwidth features, available multi-layer solutions are not a viable option since they are not compliant with such a requirement [17], [21].

Following this line of reasoning, this paper presents an innovative single-layer *RS* microstrip *EFA* radiator with horizontal polarization for automotive radars in the

77 [GHz] band. Unlike state-of-art solutions, the contour of the radiating element is modeled as a spline-shaped (*SS*) profile [33], [34], [35], [36]. Accordingly, arbitrarily-complex shapes can be yielded by acting on a limited set of geometric degrees-of-freedom (*DoF*s) to fulfil several challenging requirements on both bandwidth and radiation features. As a matter of fact, the flexibility of the proposed modeling approach enables an accurate control of the feeding phases within the operative band. Moreover, the continuous non-uniformity of the radiator width allows one to optimize the elevation *FF* features including a lowering of the sidelobe level (*SLL*), which is beneficial for reducing both near range clutter from the road surface and the multi-path interferences. Furthermore, to yield a robust/reliable design for a fruitful integration within *FMCW* automotive radars, the non-negligible material losses occurring in the *mm*-wave regime as well as the mutual coupling (*MC*) effects when integrating the antenna in the radar system composed by a linear arrangement of identical elements are taken into account by recurring to a full-wave (*FW*) modelling of the structure at hand.

Owing to the complexity of the synthesis problem at hand, the System-by-Design (*SbD*) [36], [37], [38] paradigm has been applied to solve the arising global optimization problem with a high computational efficiency. More in detail, the design of the *SS RS-EFA* (shortly in the following *SS-EFA*) has been carried out by means of a customized version of the *PSO-OK/C* method [37] based on a "low dimension" representation of the solution space and relying on the "collaboration" between a Solution Space Exploration (*SSE*) functional block based on evolutionary operators [39], [40], [41] and a Learning-By-Examples (*LBE*)-based digital twin (*DT*) of the *FW* simulator aimed at outputting fast predictions of the electromagnetic (*EM*) performance of each trial guess solution generated by the *SSE* [42]. It should be noticed that, although other *SS*-based antennas can be found in the literature [33], [34], [35], the present work deals with a completely new design in terms of radiator architecture, requirements, addressed application, and adopted synthesis methodology. More in details, *SS* layouts have been previously solely investigated to model aperture-stacked patches [33], coaxial probe-fed microstrip monopoles [34], or cavity-backed patch antennas [35] with completely different feeding mechanisms, *EM* behaviors, and operation bands. Moreover, the proposed antenna outperforms previous *SS*-based designs [33], [34], [35] in terms of beam shaping capabilities and polarization purity, since it enables a more effective control/tuning of the current density flowing from the edge feeding point. Furthermore, from the methodological point of view this is the first time, to the authors' best knowledge, that the design of a *SS*-based *mm*-wave radiator is addressed within the *SbD* framework to speed up the optimization process while considering all non-idealities of the employed materials and the presence of *MC*. The paper is organized as follows. Section II describes the *SS-EFA* geometry and

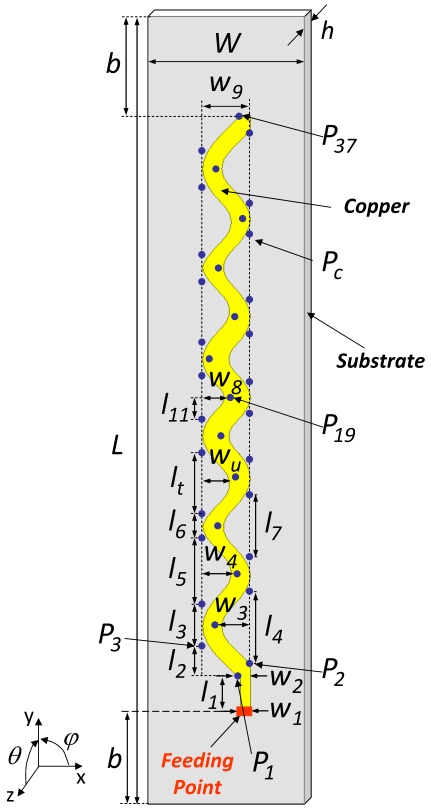

FIGURE 1. ***SS-EFA Design*** **- Sketch of the antenna geometry with its geometrical descriptors.**

it provides some theoretical insights on its *EM* working principle. The design requirements and the *SbD* procedure for the optimization of the antenna layout are detailed in Sect. III. Section IV presents selected results from the *FW*-based numerical assessment of the performance of the optimized radiator along with the experimental validation of a *SS-EFA* prototype realized on a printed circuit board (*PCB*) and measured on a custom *mm*-wave Compact Antenna Test Range (*CATR*) system. Finally, some conclusions are drawn (Sect. V).

II. SS-EFA LAYOUT AND EM WORKING PRINCIPLE

The layout of the *SS-EFA* is shown in Fig. 1. The antenna lies on the (x, y) plane and it is printed on a single-layer ground-backed Rogers $RO3003^{TM}$ high frequency ceramic-filled composite substrate with relative permittivity and loss tangent equal to $\varepsilon_r = 3.0$ and $\tan\delta = 1.0 \times 10^{-3}$, respectively, of thickness $h = 0.127$ [mm] (i.e., $h = 5$ [mil]). To take into account all non-idealities/losses occurring in the *mm*-wave band, both metallizations on the top (i.e., the radiator) and the bottom (i.e., the ground plane) layers are modeled as copper with conductivity $\sigma = 2.5 \times 10^7$ [S/m], thickness $\tau = 25 \times 10^{-6}$ [m], and roughness $\rho = 1.3 \times 10^{-6}$ [m].

The antenna is fed from the bottom edge with a tapered microstrip feeding line of length l_1, having controllable

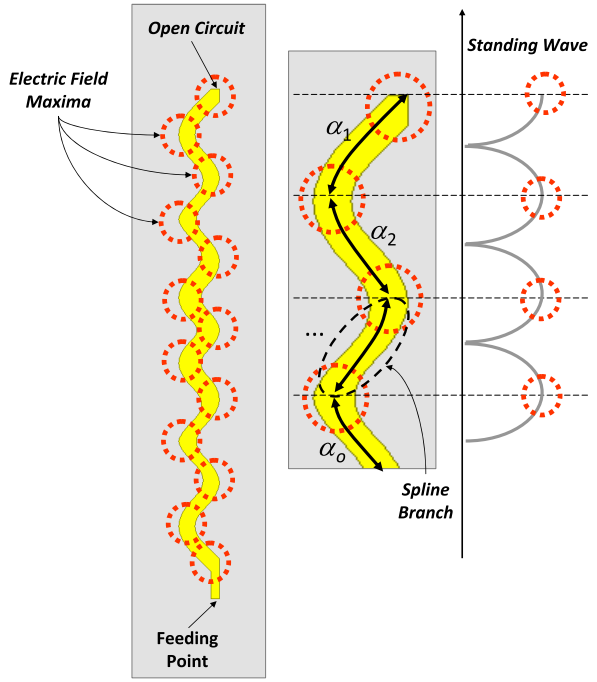

FIGURE 2. ***SS-EFA Working Principle*** **- Pictorial representation of the *SW* excited within the *SS-EFA* structure.**

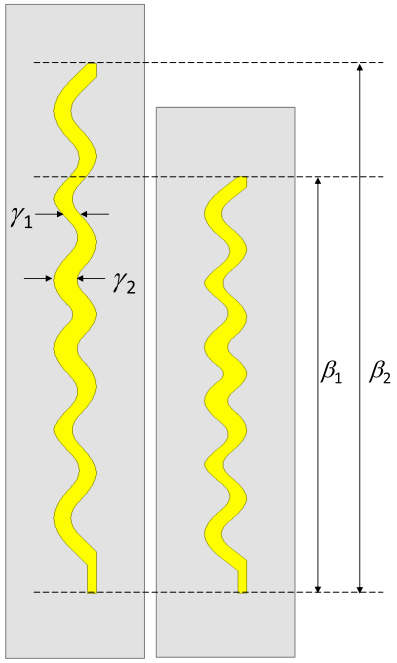

FIGURE 3. ***SS-EFA Working Principle*** **- Sketch of two non-uniform width ($\gamma_1 \neq \gamma_2$) and different length ($\beta_1 \neq \beta_2$) *SS-EFA*s.**

starting, w_1, and ending, w_2, widths to yield a proper 50 [Ω] impedance matching over the complete working band.[1] As for the shape of the radiator, which is connected to the feeding line, an innovative non-uniform *SS* profile is adopted [33], [34], [35], [36] since (*i*) there is the possibility to model complex geometries for fitting multiple and sometimes contrasting requirements on both bandwidth and far-field (*FF*) features with a reduced set of properly-tuned *DoF*s; (*ii*) the absence of sharp edges is a recipe to mitigate the fringing effects that enhance the *MC* between the adjacent elements of the final radar layout [33]. More in detail, Bézier spline basis functions [33], with $C = 37$ control points, $\underline{P} = \{P_c = (x_c, y_c)\,;\, c = 1, \ldots, C\}$ (Fig. 1), are adopted to shape the contour of the *SS-EFA*.

The spline radiator is terminated on the opposite side of the feeding point with an open circuit (i.e., no matched load) so that a resonant behavior is yielded by exciting a standing wave (*SW*) within the microstrip structure (Fig. 2). As a matter of fact, the maxima of the electric field occur in correspondence of the bending corners of the *SS-EFA* that, in turn, correspond to the positions of the *SW* maxima (Fig. 2). To afford the desired resonating behavior, the surface current in each spline branch must be tuned in-phase so that the *FF* radiated contributions constructively add in the antenna broadside direction [i.e., $(\theta_0, \varphi_0) = (0, 0)$ [deg] - Fig. 1]. Towards this end, the electrical length of each o-th ($o = 1, \ldots, O$; $O \triangleq \frac{C-1}{3} \rightarrow O = 12$) intermediate spline segment, α_o, must be properly designed so that the current, injected from the feeding point and flowing up to the open circuit, is equally-phased at each radiating location (Fig. 2) despite the single-point edge-feeding mechanism.

It is also worth pointing out that thanks to the continuously non-uniform width of the *SS* metallization (e.g., $\gamma_1 \neq \gamma_2$ - Fig. 3), it is possible to excite a tapered current distribution within the *EFA* to perform beam shaping and obtain a lower *SLL* with respect to a uniform-width profile. Such a *FF* feature is highly desirable in automotive applications since it reduces the interferences from both the asphalt and the sky, thus leading to a more robust and reliable target detection/location and *DoA* estimation. Clearly, the non-uniform width of the spline profile cannot be arbitrarily set, and its local tuning must be optimized to define a suitable trade-off between the *SLL* and other important performance indexes (e.g., impedance matching).

As for the *FF* half-power beamwidth (*HPBW*), which affects the angular resolution of the automotive radar along the elevation plane, it is controlled by the overall length of the *SS* radiator. Indeed, longer structures exhibit narrower *HPBW*s (e.g., $\beta_2 > \beta_1 \rightarrow HPBW|_{\beta_2} < HPBW|_{\beta_1}$ - Fig. 3) and vice-versa, because of the different aperture size of the equivalent linear array.

In order to guarantee geometric/electric symmetry by also keeping low the number of problem descriptors, only one half of the spline curve (i.e., $\{P_c;\, c = 1, \ldots, 19\}$ - Fig. 1) is optimized, while the coordinates of the second half of the control points (i.e., $\{P_c;\, c = 20, \ldots, C\}$ - Fig. 1) are automatically derived with a mirroring operation with respect

[1] In order to maximize the power flow into the *SS* series-fed radiating structure, a tapered input section is adopted and its geometric descriptors w_1 and w_2 are included in the design variables, as detailed in the following.

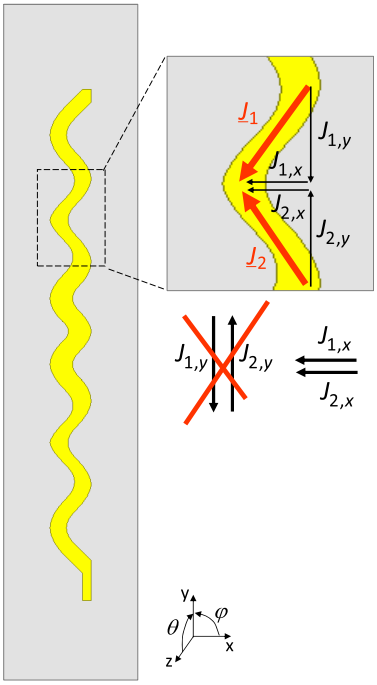

FIGURE 4. ***SS-EFA Working Principle*** **- Pictorial representation of the behavior of the surface current density.**

to the horizontal axis (i.e., x-axis - Fig. 1). Enforcing such a symmetry allows one to also yield a lower *BDD* and a higher similarity of the left/right side-lobes on the vertical plane (i.e., $\varphi = 90$ [deg] - Fig. 1).

Finally, it is important to point out that despite the unconventional and non-uniform shaping of the radiating element, the *SS-EFA* radiates, as required, a linearly polarized field along the horizontal direction with a high polarization purity. As a matter of fact, the surface current density distributions excited within each pair of adjacent spline branches (e.g., $\underline{J}_1 = J_{1,x}\widehat{\underline{x}} + J_{1,y}\widehat{\underline{y}}$ and $\underline{J}_2 = J_{2,x}\widehat{\underline{x}} + J_{2,y}\widehat{\underline{y}}$ - Fig. 4) exhibit in-phase x-components (e.g., $J_{1,x}$ and $J_{2,x}$ - Fig. 4) and out-of-phase y-components (e.g., $J_{1,y}$ and $J_{2,y}$ - Fig. 4) so that, while the x-components constructively sum, the y ones cancel out and the *EM* source turns out to be x-polarized.

III. DESIGN PROCESS

The *SS-EFA* has been synthesized to provide a suitable matching so that $|S_{11}(f)| \leq S_{11}^{th}$ ($S_{11}^{th} = -10$ [dB]) within the frequency range $\Delta f = [f_{\min}, f_{\max}]$ [24], $f_{\min}$ and $f_{\max}$ being the minimum ($f_{\min} = 76$ [GHz]) and the maximum ($f_{\max} = 78$ [GHz]) working frequency, respectively. Concerning the radiation features, the *SLL*, the *HPBW*, and the *BDD* on the vertical plane have been required to comply with the following requirements: $SLL(f) \leq SLL^{th}$ ($SLL^{th} = -15$ [dB]), $HPBW(f) \leq HPBW^{th}$ ($HPBW^{th} = 18$ [deg]), and $BDD(f) \leq BDD^{th}$ ($BDD^{th} = 2$ [deg]).[2]

[2]The *BDD* is defined as $BDD(f) = |\theta_{\max}(f)|$, where $\theta_{\max}(f) = \arg\left\{\max_\theta\left[G(f, \theta, \varphi)|_{\varphi=90\,[\text{deg}]}\right]\right\}$, $G(f, \theta, \varphi)|_{\varphi=90\,[\text{deg}]}$ being the gain pattern function in the vertical (elevation) plane of the antenna (Fig. 1).

TABLE 1. Radar antenna requirements.

Feature	*Requirement*
Operating Band	$f \in [f_{\min}, f_{\max}] = [76, 78]$ [GHz]
Reflection Coefficient	$S_{11} \leq S_{11}^{th} = -10$ [dB]
Sidelobe Level	$SLL \leq SLL^{th} = -15$ [dB]
Half-Power Beamwidth	$HPBW \leq HPBW^{th} = 18$ [deg]
Beam Direction Deviation	$BDD \leq BDD^{th} = 2$ [deg]
Polarization Ratio	$PR \geq PR^{th} = 20$ [dB]

Furthermore, the polarization ratio (*PR*) is required to be $PR(f) \geq PR^{th}$ ($PR^{th} = 20$ [dB]).[3] For the sake of clarity, all design objectives/targets are reported in Tab. 1.

To yield a robust design and to enable a reliable prediction of the *EM* behavior of the elementary radiator when integrated in an automotive radar system,[4] it has been synthesized not alone, but within a linear arrangement of $N = 5$ identical half-wavelength ($W = \frac{\lambda_0}{2} = 1.95 \times 10^{-3}$ [m], λ_0 being the free-space wavelength at the central frequency $f_0 = 77$ [GHz]) spaced *SS-EFA*s ($W_s = 15$ [mm] - Fig. 5), which has been modeled with a *FW* finite model. More specifically, the synthesis has been aimed at optimizing all performance indexes for the central embedded element, while the surrounding $(N-1)$ replicas have been terminated on 50 [Ω] matched loads (Fig. 5).

Owing to the computational complexity of the synthesis problem at hand, the design has been efficiently carried out within the *SbD* framework [36], [37], [38]. As a matter of fact, the *SbD* has recently emerged as an innovative paradigm enabling an effective and computationally-efficient use of global optimizers for the solution of complex *EM* synthesis problems. Accordingly, the computational burden (resulting from the need for iterated accurate *FW*-assessments of the finite structure in Fig. 5) is addressed by suitably selecting and integrating *functional blocks* comprising problem-dependent, efficient, and reliable prediction and optimization strategies [37]. More specifically, the customization of the *SbD* to the synthesis problem at hand starts from a "smart" representation of the *SS-EFA* solution space in the so-called *"Problem Formulation"* functional block [37]. Towards this end, the following $K = 20$ descriptors $\underline{\chi} = \{\chi_k;\ k = 1, \ldots, K\}$ where $\chi_k = l_k$ ($k = 1, \ldots, T$; $T = 11$) and $\chi_k = w_{k-T}$ ($k = T+1, \ldots, T+U$; $U = 9$) (Fig. 1) have been considered instead of using the coordinates of the control points of the spline contour (i.e., $K = 2 \times C \rightarrow K = 74$). The synthesis problem has been then reformulated as a minimization one by defining the following customized cost function

$$\Phi\left(\underline{\chi}\right) = \alpha_{S_{11}}\Phi_{S_{11}}\left\{\underline{\chi}\right\} + \alpha_{SLL}\Phi_{SLL}\left\{\underline{\chi}\right\} + \alpha_{HPBW}$$

[3]The *PR* is defined as $PR(f) = \left|\frac{E_x(f, \theta=0)}{E_y(f, \theta=0)}\right|$, $E_{x/y}$ being the x/y-components of the *FF* electric field, respectively.

[4]*FMCW* multiple-input multiple-output (*MIMO*) automotive radars are generally implemented as properly-spaced arrangements of both transmitting and receiving elementary radiators connected to a single driving chip [1], [43], [44].

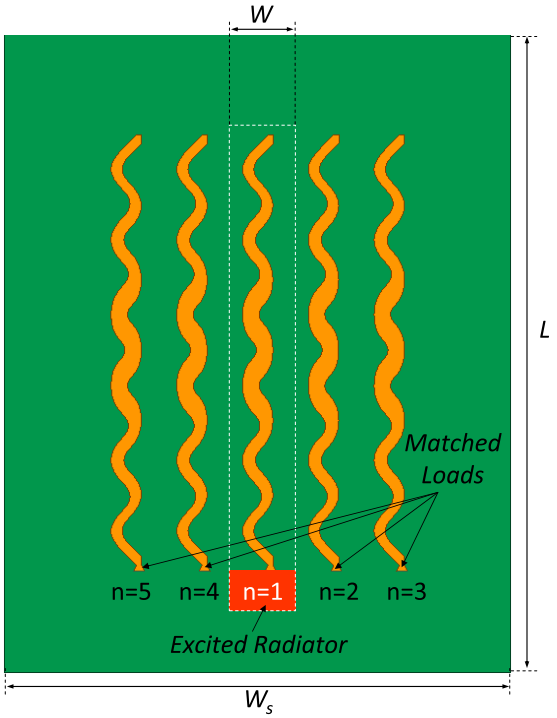

FIGURE 5. *Numerical Assessment* ($N = 5$) - Screenshot of the *SbD*-synthesized optimal *SS-EFA* radiator layout embedded within a $N = 5$ linear array of identical $\frac{\lambda_0}{2}$-spaced replicas.

$$\times \Phi_{HPBW}\left\{\underline{\chi}\right\} + \alpha_{BDD}\Phi_{BDD}\left\{\underline{\chi}\right\} + \alpha_{PR}\Phi_{PR}\left\{\underline{\chi}\right\}, \tag{1}$$

where

$$\Phi_{S_{11}}\left\{\underline{\chi}\right\} = \frac{1}{Q}\sum_{q=1}^{Q}\mathcal{H}\left\{\frac{S_{11}\left(f_q,\,\underline{\chi}\right) - S_{11}^{th}}{\left|S_{11}^{th}\right|}\right\}, \tag{2}$$

$$\Phi_{SLL}\left\{\underline{\chi}\right\} = \frac{1}{Q}\sum_{q=1}^{Q}\mathcal{H}\left\{\frac{SLL\left(f_q,\,\underline{\chi}\right) - SLL^{th}}{\left|SLL^{th}\right|}\right\}, \tag{3}$$

$$\Phi_{HPBW}\left\{\underline{\chi}\right\} = \frac{1}{Q}\sum_{q=1}^{Q}\mathcal{H}\left\{\frac{HPBW\left(f_q,\,\underline{\chi}\right) - HPBW^{th}}{HPBW^{th}}\right\}, \tag{4}$$

$$\Phi_{BDD}\left\{\underline{\chi}\right\} = \frac{1}{Q}\sum_{q=1}^{Q}\mathcal{H}\left\{\frac{BDD\left(f_q,\,\underline{\chi}\right) - BDD^{th}}{BDD^{th}}\right\}, \tag{5}$$

and

$$\Phi_{PR}\left\{\underline{\chi}\right\} = \frac{1}{Q}\sum_{q=1}^{Q}\mathcal{H}\left\{\frac{PR^{th} - PR\left(f_q,\,\underline{\chi}\right)}{PR^{th}}\right\} \tag{6}$$

are the impedance matching, the *SLL*, the *HPBW*, the *BDD*, and the *PR* cost terms quantifying the mismatch with respect to the corresponding user-defined thresholds. Moreover, $\underline{\alpha} = \left\{\alpha_{S_{11}};\, \alpha_{SLL};\, \alpha_{HPBW};\, \alpha_{BDD};\, \alpha_{PR}\right\} \geq 0$ are real valued weights, while $\mathcal{H}\{\xi\} = \xi$ if $\xi \geq 0$ and $\mathcal{H}\{\xi\} = 0$, otherwise, is the ramp function. Finally, the frequency band Δf has been uniformly sampled into $Q = 41$ points, $\{f_q = f_{\min} + (q-1)\,\frac{(f_{\max}-f_{\min})}{(Q-1)};\, q = 1, \ldots, Q\}$, for constraining the fulfilment of the requirements in the whole bandwidth.

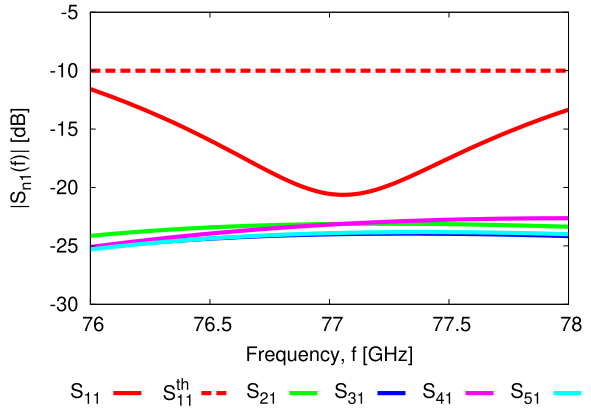

FIGURE 6. *Numerical Assessment* ($N = 5$) - Magnitude of the reflection coefficient, $|S_{11}(f)|$ ($n = 1$), and of the scattering coefficients, $|S_{n1}(f)|$ ($n = 2, \ldots, N$), of the central embedded element ($n = 1$) versus the frequency f ($f \in \Delta f$) for the linear arrangement in Fig. 5.

The multi-modal nature of the cost function (1) as well as the impossibility to derive closed-forms expressions of its derivatives prohibit the exploitation of fast local-search gradient-descent algorithms. On the other hand, a global optimization using standard evolutionary algorithms, although guaranteeing an effective exploration of the solution space without being trapped into local minima, would result in a very high computational load [37]. Owing to such considerations, the minimization of (1) has been carried out with a properly customized version of the *PSO-OK/C SbD* method [37] leveraging on the "collaboration" between the *SSE* functional block relying on the Particle Swarm Optimization (*PSO*) operators [41] and a fast *DT* based on the Ordinary Kriging (*OK*) *LBE* technique [42]. The meta-level control parameters of the *PSO* have been set according to the literature guidelines [37]: $V = 10$ (V being the swarm size), $I = 200$ (I being the maximum number of iterations), $\omega = 0.4$ (ω being the inertial weight), and $\mathcal{C}_1 = \mathcal{C}_2 = 2.0$ ($\mathcal{C}_1$ and $\mathcal{C}_2$ being the social and the cognitive acceleration coefficient, respectively).

As for the *OK* prediction model, the fast surrogate of the *FW* simulator has been trained with $S_0 = 100$ training samples generated *off-line* according to the Latin Hypercube Sampling (*LHS*) strategy [37], while $S_{upd} = 200$ "reinforcement training" *FW* simulations have been performed *on-line* by the *PSO-OK/C* to adaptively enhance the *DT* accuracy during the iterative minimization of (1).

The solution, $\underline{\chi}^{(opt)}$, outputted by the *SbD* at the convergence [i.e., $\Phi\left(\underline{\chi}^{(opt)}\right) = 0$] that fulfils all the user-defined requirements (letting $\underline{\alpha} = 1.0$), as it can be inferred in Sect. IV-A, is reported in Tab. 2, while the *CAD* model of the corresponding *SS-EFA* layout (surrounded by four identical replicas) is shown in Fig. 5, the total

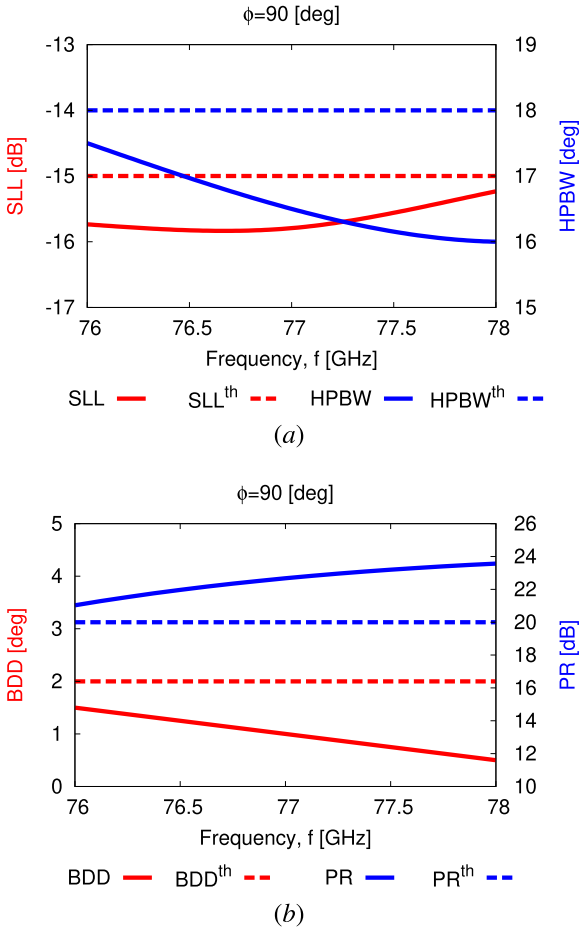

FIGURE 7. ***Numerical Assessment*** **($N = 5$, $n = 1$, $\varphi = 90$ [deg]) - Behavior of (*a*) *SLL* and *HPBW* and (*b*) *BDD* and *PR* versus the frequency f ($f \in \Delta f$).**

TABLE 2. Values of the descriptors of the *SbD*-synthesized *SS-EFA* layout.

Geometrical Descriptors [m]			
w_1	3.26×10^{-4}	l_2	7.57×10^{-4}
w_2	1.46×10^{-4}	l_3	5.27×10^{-4}
w_3	7.57×10^{-4}	l_4	1.51×10^{-3}
w_4	7.57×10^{-4}	l_5	1.51×10^{-3}
w_5	6.90×10^{-4}	l_6	6.47×10^{-4}
w_6	6.90×10^{-4}	l_7	1.38×10^{-3}
w_7	5.52×10^{-4}	l_8	1.38×10^{-3}
w_8	5.52×10^{-4}	l_9	1.00×10^{-3}
w_9	9.03×10^{-4}	l_{10}	1.10×10^{-3}
l_1	1.80×10^{-4}	l_{11}	5.22×10^{-4}

length of the radiator being equal to $L = l_1 + 2 \times (b + l_2 + l_3 + l_5 + l_6 + l_8 + l_9 + l_{11}) \rightarrow L = 18.9 \times 10^{-3}$ [m] since $b = 3 \times 10^{-3}$ [m] is a fixed offset from the bottom and the top edges of the substrate (Fig. 1).

It is worthwhile to point out that the time saving Δt_{sav} [$\Delta t_{sav} \triangleq \frac{\Delta t_{PSO} - \Delta t_{SbD}}{\Delta t_{PSO}} = \frac{(V \times I) - (S_0 + S_{upd})}{(V \times I)}$] enabled here by the *SbD* strategy [37] with respect to a standard optimization that exclusively relies on iterated *FW* calls (i.e., $V \times I$) [40] amounts to $\Delta t_{sav} = 85\%$. As a matter of fact, the

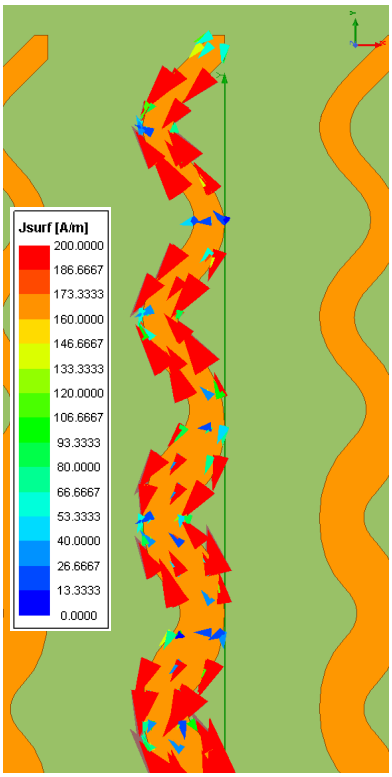

FIGURE 8. ***Numerical Assessment*** **($N = 5$, $n = 1$) - Screenshot of the simulated surface current density at $f = f_0$.**

PSO-OK/C method only requires to simulate the initial S_0 training designs and the S_{upd} configurations adaptively selected during the optimization, while relying on almost real-time predictions of (1) for all the remaining trial particles generated throughout the iterative minimization procedure [37]. Quantitatively, the synthesis has been completed in $\Delta t_{SbD} \approx 2.25 \times 10^2$ [hours], while $\Delta t_{PSO} = 1.5 \times 10^3$ [hours] would be the overall time expense for a standard (non-*SbD*) *PSO*-based optimization.[5]

IV. PERFORMANCE ASSESSMENT

The goal of this section is twofold. On the one hand, to present the results of a careful assessment of the *FW*-simulated *EM* features of the synthesized *SS-EFA* (Sect. IV-A). On the other hand, to show the outcomes from the experimental validation, carried out on a *PCB*-manufactured prototype, to confirm the *FW* simulations (Sect. IV-B) towards the use of the proposed *mm*-wave radiator in automotive radar applications.

A. NUMERICAL ASSESSMENT

Figure 6 shows the behavior of the reflection coefficient of the central ($n = 1$) embedded element within the linear arrangement of $N = 5$ identical *SS-EFA*s simulated by means of the Ansys *HFSS FW* solver [45] (Fig. 5). As it can be inferred, the antenna correctly resonates within the operative

[5]The average time cost of a single *FW* simulation of the finite-size model in Fig. 5 is equal to $\Delta t_{FW} \approx 45$ [min] on a desktop *PC* with Intel(R) Core(TM) i7-4790 *CPU* @ 3.60 [GHz] and 32 [GB] of *RAM* memory.

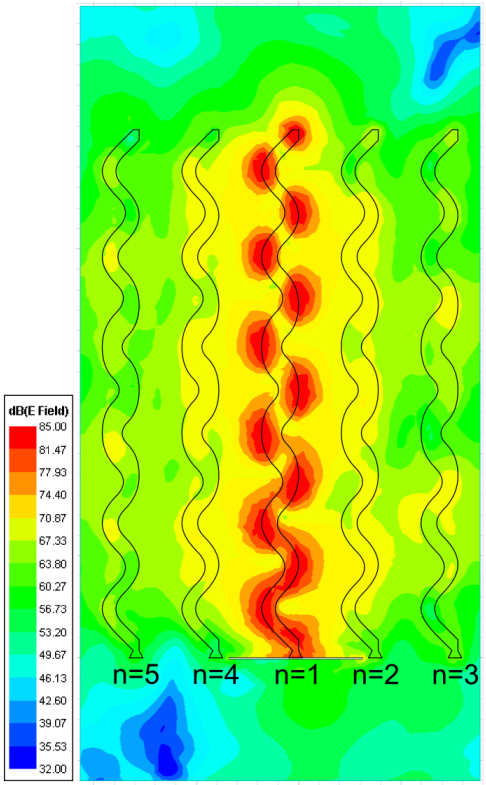

FIGURE 9. *Numerical Assessment* ($N = 5$, $n = 1$) - Screenshot of the magnitude of the total electric field, $|\mathbf{E}(x, y; f_0)|$, computed over a plane parallel to the (x, y) plane far $z = \frac{\lambda_0}{20}$ from the *SS-EFA* surface, at $f = f_0$.

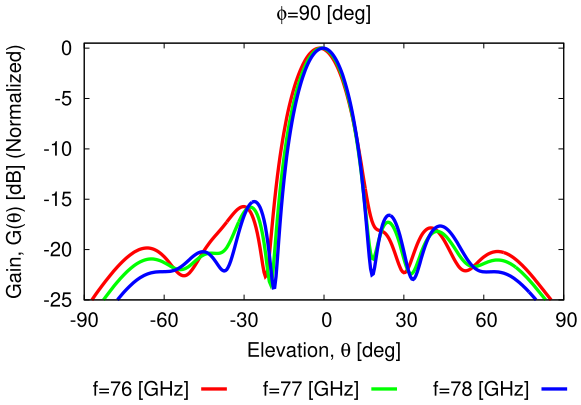

FIGURE 10. *Numerical Assessment* ($N = 5$, $n = 1$, $\varphi = 90$ [deg]) - Embedded gain pattern at $f = f_{\min}$, $f = f_0$, and $f = f_{\max}$.

band being $|S_{11}(f)| \leq -11.6$ [dB] for $f \in \Delta f$. Moreover, the optimized *SS-EFA* provides a suitable inter-element isolation as indicated by the magnitude of the scattering coefficients [i.e., $|S_{n1}(f)| \leq -22.6$ [dB] $(n = 2, \ldots, N)$].

As for the *FF* features of the *SbD*-layout, the curves in Fig. 7(*a*) show that $SLL(f) \leq -15.3$ [dB] and $HPBW(f) \leq 17.5$ [deg] for $f \in \Delta f$ (i.e., both *SLL* and *HPBW* comply with the requirement). Moreover, the synthesized radiator turns out to be fully-compliant in terms of beam pointing stability regardless of the adopted edge feeding mechanism as confirmed by the *BDD* values (i.e., $BDD \leq 1.5$ [deg]) in Fig. 7(*b*).

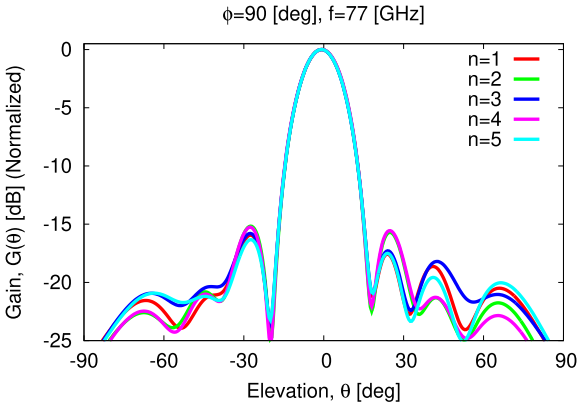

FIGURE 11. *Numerical Assessment* ($N = 5$, $\varphi = 90$ [deg], $f = f_0$) - Comparison of the embedded gain patterns of all elements ($n = 1, \ldots, N$) forming the linear arrangement in Fig. 5.

On the other hand, it should be very interesting for the readers to observe that the arising *SS-EFA* structure radiates a linearly (horizontal) polarized field with high polarization purity despite its smooth/non-uniform profile (Fig. 1). Indeed, it turns out that $PR(f) \geq 21$ [dB] for $f \in \Delta f$ [Fig. 7(*b*)] as a consequence of the distribution of the surface current (Fig. 8) that follows the theoretically-expected configuration sketched in Fig. 4. An overall x-polarized source is excited in correspondence with each radiating location of the resonant structure shown in Fig. 9 where the near-field (*NF*) distribution of the magnitude of the electric field, $|\mathbf{E}(x, y; f_0)|$, computed on a $(5W \times L)$-sized plane at height $z = \frac{\lambda_0}{20}$ from the *SS-EFA*, is reported. This latter plot highlights the resonant behavior of the synthesized structure, the field being maximum at fixed and equally-spaced positions. As expected, such maxima, which correspond to those of the *SW* excited within the structure, arise on the bends of the spline contour and they generate in-phase radiation contributions that result in a suitable beam shaping and a pointing stability within the working band Δf as confirmed by the simulated *FF* pattern at $f = f_{\min}$, $f = f_0$, and $f = f_{\max}$ in Fig. 10. Moreover, the magnitude of the coupling field in the adjacent radiators ($n = 2$ and $n = 4$) is always 14.8 [dB] lower than in the driven element ($n = 1$), the arising *MC* being always acceptable as indicated by the corresponding scattering coefficients (i.e., $|S_{21}(f_0)| = -23.1$ [dB] and $|S_{41}(f_0)| = -23.2$ [dB] - Fig. 6). For completeness, the embedded pattern of the central element is compared to that of the (non-optimized) neighboring elements ($n = 2, \ldots, N$) in Fig. 11. As expected, some differences between the elements can be observed because of the small dimension of the simulated array (Fig. 5). However, it turns out that such discrepancies are quite limited thanks to the low coupling among adjacent radiators, thus further indicating the suitability of the designed radiator for a successive integration within *FMCW* radars.

In order to further demonstrate the beam-shaping capabilities of the proposed optimization strategy, let us consider the case of an antenna design optimized without enforcing

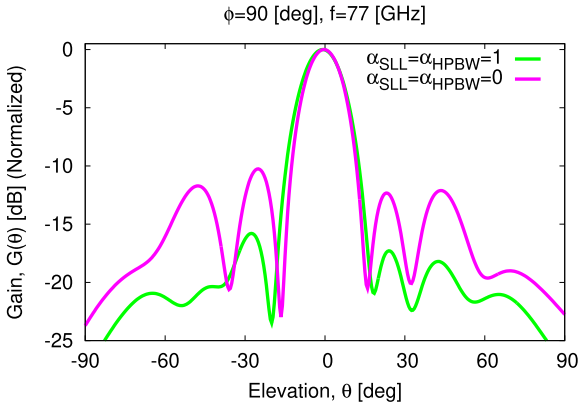

FIGURE 12. ***Numerical Assessment*** **($N = 5$, $n = 1$, $\varphi = 90$ [deg], $f = f_0$) - Comparison of the embedded gain pattern when enabling ($\alpha_{SLL} = \alpha_{HPBW} = 1.0$) or disabling ($\alpha_{SLL} = \alpha_{HPBW} = 0.0$) the optimization of the *SLL* and the *HPBW*.**

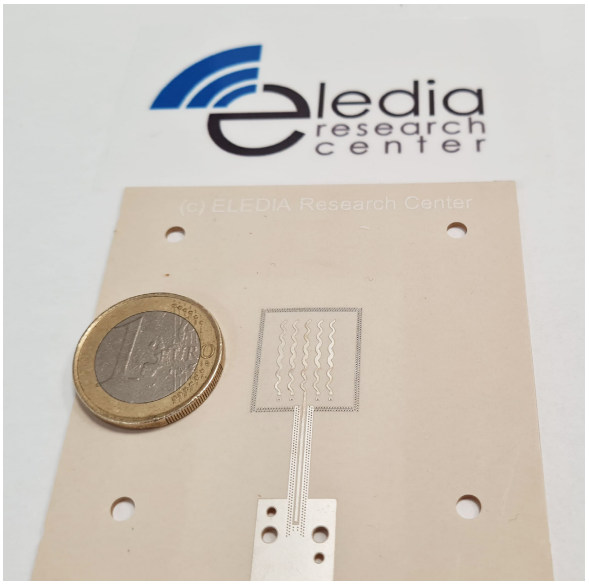

(*a*)

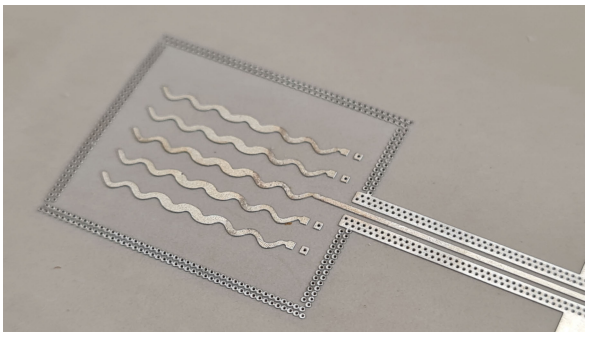

(*b*)

FIGURE 13. ***Experimental Assessment*** **- Picture of (*a*) the *SS-EFA* prototype and (*b*) a zoom on the radiating part.**

constraints on the *SLL* and *HPBW*. Towards this end, a second optimization has been performed by letting the two weights

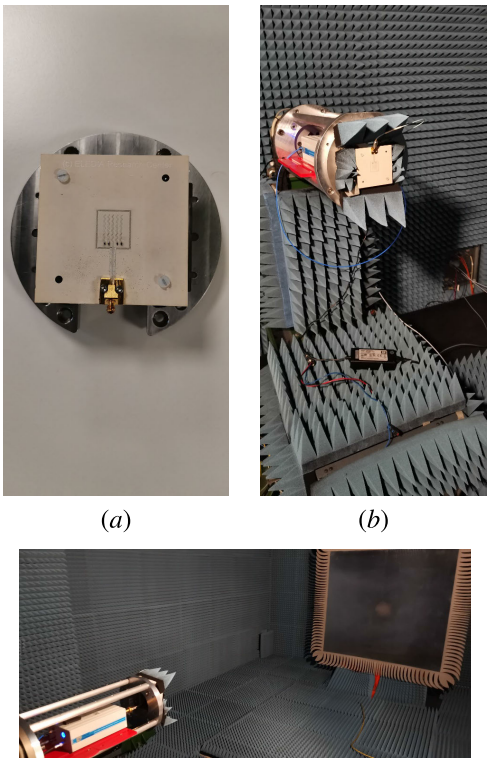

(*a*) (*b*)

(*c*)

FIGURE 14. ***Experimental Assessment*** **- Picture of (*a*) the *AUT*, (*b*) the *CATR* positioner, and (*c*) the whole measurement setup.**

associated to such indexes equal to $\alpha_{SLL} = \alpha_{HPBW} = 0.0$, thus "disabling" the corresponding cost terms (3)(4) in the cost function (1). The result is shown in Fig. 12 in terms of pattern of the central element at $f = f_0$. As it can be observed, the absence of specific constraints resulted in remarkably higher side-lobes (i.e., $SLL\,(f_0)|_{\alpha_{SLL}=\alpha_{HPBW}=0.0} = -10.2$ [dB] vs. $SLL\,(f_0)|_{\alpha_{SLL}=\alpha_{HPBW}=1.0} = -15.8$ [dB] - Fig. 12). As a consequence, a narrower beamwidth has been yielded (i.e., $HPBW\,(f_0)|_{\alpha_{SLL}=\alpha_{HPBW}=0.0} = 15.0$ [deg] vs. $HPBW\,(f_0)|_{\alpha_{SLL}=\alpha_{HPBW}=1.0} = 16.5$ [deg] - Fig. 12). On the other hand, the same beam pointing accuracy has been kept (i.e., $BDD|_{\alpha_{SLL}=\alpha_{HPBW}=0.0} \leq 1.5$ [deg]).

Finally, it is worth comparing the proposed antenna with other designs available in the scientific literature. Towards this end, Table 3 summarizes the main features of several state-of-art competitive solutions complying with the two main requirements of (*a*) horizontal polarization and (*b*) single-layer layout. As expected, it is not possible to find a unique "winning" design in terms of all key performance indicators (*KPI*s), since each technological solution could in principle represent the best trade-off for a given application (i.e., project requirements/constraints). However, it turns out that there are several positive and supporting aspects motivating the proposal of the antenna at hand. By neglecting the *HPBW* since (*i*) it is inversely proportional to the length of the radiating structure (Tab. 3) and (*ii*) it is an application-dependent feature, it appears that the proposed

TABLE 3. Comparison between the proposed antenna and other designs with single-layer structure and horizontal polarization in the recent literature. Gain, *SLL*, *HPBW*, *PR*, and radiation efficiency are reported at $f = f_0$.

Ref.	Radiator Type	Feeding	f_0 [GHz]	*FBW* [%]	*BDD* [deg]	Gain [dBi]	*SLL* [dB]	*HPBW* [deg]	*PR* [dB]	Length [λ_0]
This Work	Spline-Shaped	*EFA*	77.0	2.6	≤ 1.5	13.8	-15.8	16.5	22.7	4.9
[31]	Microstrip Line	*EFA*	28.0	4.6	N.A.	10.7	-15.8	16	18.4	6.0
[32]	Asymmetric Trapezoidal Microstrip	*EFA*	78.0	13.0	≤ 2.2	10.4	-16.1	22.7	N.A.	3.4
[22]	Slotted *SIW*	*EFA*	79.0	5.4	*N.A.*	6.5	-24.0	34.0	30.1	2.7
[30]	Periodic Microstrip *LWA*	*EFA*	22.5	69.6	≤ 55.0	12.9	-13.3	10.5	N.A.	5.3
[13]	Linear Grid Array	*CFA*	24.2	1.2	*N.A.*	19.0	-20.0	5.0	40.0	11.6
[26]	Slotted *SIW*	*CFA*	24.0	1.7	0.0	24.0	-24.5	4.6	*N.A.*	15.6
[9]	Microstrip Array	*CFA*	27.0	50.6	N.A.	12.5	-28.4	25.0	22	2.7

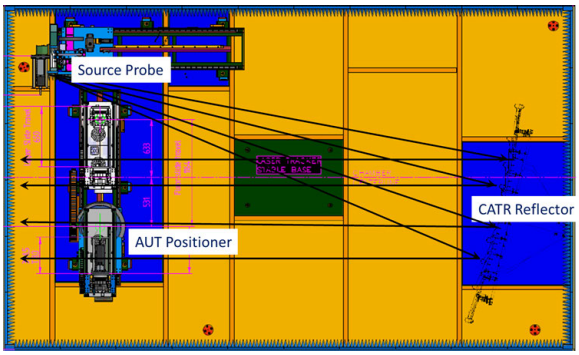

FIGURE 15. ***Experimental Assessment*** **- Sketch of the measurement scenario.**

design overcomes state-of-the-art *EFA* alternatives in several fundamental *KPI*s. For instance, the performance comparison with the solution in [31] shows that the proposed design exhibits higher gain (+29%) and *PR* (+23%) with the same *SLL*. It also outperforms the design in [32] in terms of gain (+33%) and *BDD* (−32%). Moreover, when compared to the solution in [22], it shows a remarkably higher gain (+112%) with a simpler manufacturing process not involving vias (as in slotted *SIWs* [22]). Otherwise, higher gain (+7%) and lower *SLL* (−19%) are observed with respect to the leaky-wave antenna (*LWA*) in [30], which is meant for performing beam scanning with frequency and therefore providing an unsuitable *BDD* performance for the targeted automotive application of this work. For the sake of completeness, some *CFA* solutions have been reported as well (Tab. 3). With respect to [13] and [26], the proposed *SS-EFA* provides a larger bandwidth (+117% vs. [13] and +53% vs. [26]), while it yields a higher gain (+10%) when compared to [9]. Moreover, it is worth remarking that edge-feeding is a highly desirable feature in radar applications where the radiators must be arranged into closely-packed/single-layer layouts in which simple routing connections to the controlling chipset are mandatory. Therefore, the proposed antenna may be a better (if not the only "physically admissible") technological choice with respect to such center-fed designs.

B. EXPERIMENTAL VALIDATION

A prototype of the *SS-EFA* has been fabricated through *PCB* manufacturing on a substrate of size 70 × 70 [mm]

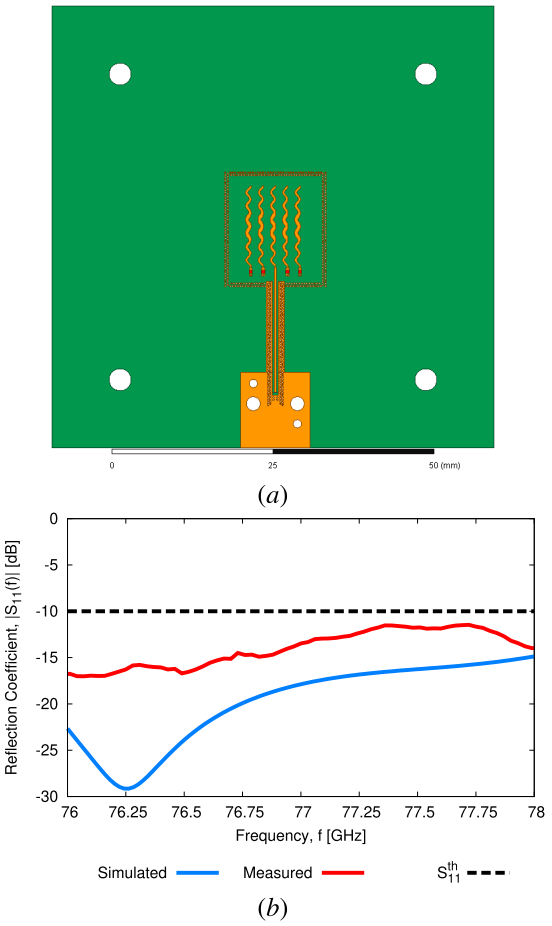

FIGURE 16. ***Experimental Assessment*** **- (*a*) Simulated pre-prototyping layout and (*b*) comparison between simulated and measured input reflection coefficient of the central element ($n = 1$).**

(Fig. 13). The bottom ground plane has been stacked on a 1 [mm]-thick *FR-4* layer to enhance the mechanical robustness and rigidity of the antenna under test (*AUT*). Moreover, four holes, 3.5 [mm] in diameter, have been drilled at the corners of a square of side 48.5 [mm] to fix the *AUT* on the measurement support by means of plastic screws [Fig. 13(*a*) and Fig. 14(*a*)]. The central radiator ($n = 1$) has been fed by using a Rosemberger *01K80A-40ML5* connector installed without soldering at the bottom edge of the *AUT*

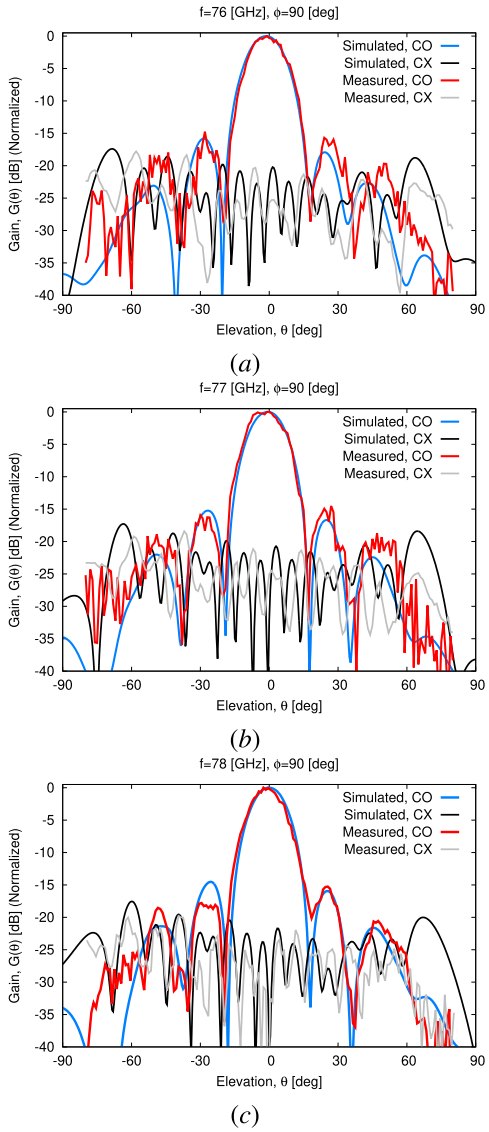

FIGURE 17. ***Experimental Assessment*** **($N = 5$, $n = 1$, $\varphi = 90$ [deg]) - Comparison between simulated and measured co-polar (*CO*) and cross-polar (*CX*) embedded element patterns at (*a*) $f = f_{\min}$, (*b*) $f = f_0$, and (*c*) $f = f_{\max}$.**

substrate [Fig. 14(*a*)]. The neighboring *SS* elements (i.e., $n = 2, \ldots, N$) have been terminated on *MCR1* compact thick film chip resistors (series 0402) acting as matched loads. Moreover, the active and the dummy radiators as well as the feeding line have been surrounded by a double set of interleaved vias to suppress the insurgence of undesired surface currents due to the electrically-large dimension of the *PCB* [Fig. 13(*b*)].

The measurement set-up [Figs. 14(*b*)-14(*c*)] has been composed by a *mm*-wave *CATR* system within an Asysol anechoic chamber (Fig. 15) suitable for antenna measurements up to 170 [GHz].

Figure 16(*a*) shows the simulated layout in *Ansys HFSS* (modeling the prototype of Fig. 13), while a comparison between the simulated and the measured input reflection coefficient of the central element ($n = 1$) is shown in Fig. 16(*b*). As it can be observed, the antenna properly resonates in the entire operation band, being $|S_{11}(f)|^{meas} \leq -11.4$ [dB], $f \in \Delta f$.[6] Figure 17 shows the *SS-EFA* co-polar (*CO*) and cross-polar (*CX*) gain patterns measured along the $\varphi = 90$ [deg]-cut at the minimum [$f = f_{\min}$ - Fig. 17(*a*)], the central [$f = f_0$ - Fig. 17(*b*)], and the maximum [$f = f_{\max}$ - Fig. 17(*c*)] operating frequencies. As it can be observed, the *FF* patterns of the prototype well match the simulated ones. More specifically, there is a very good agreement in both the co-polar main lobe region and the first left/right sidelobes. Some slight deviations, occurring especially in the lateral sidelobes, are probably due to both prototype manufacturing inaccuracies and measurement tolerances whose impact is certainly significant in the *mm*-wave regime. Moreover, these experimental results confirm the *FW*-predicted *SLL* performance since $SLL^{meas} \leq -14.5$ [dB], for $f \in \Delta f$ (Fig. 17). Similarly, the measured *CX* patterns assess the high polarization purity of the proposed *SS-EFA* radiating element. As a matter of fact, the normalized *CX* pattern is always lower than -18 [dB] for $\theta \in [-90, 90]$ [deg] and lower than -25 [dB] along the broadside, for $f \in \Delta f$ (Fig. 17). Finally, the measured realized gain is equal to $RG^{meas}(f_{\min}) = 11.8$ [dB], $RG^{meas}(f_0) = 13.2$ [dB], and $RG^{meas}(f_{\max}) = 14.0$ [dB], at the minimum, central, and maximum frequencies, respectively.

V. CONCLUSION

A novel radiating element for 77 GHz automotive radars has been proposed that relies on a spline-based modeling to yield a high geometric flexibility with a reduced number of *DoF*s, while enabling the fitting of the several contrasting requirements on bandwidth and *FF* features. The synthesized layout, which has been efficiently obtained by means of a customized *SbD* approach, provides a proper input impedance matching, a high isolation, a suitable *SLL*/*HPBW* as well as a high polarization purity and a stable beam pointing over frequency regardless of the edge-feeding mechanism. The experimental assessment, carried out in a *CATR mm*-wave system on a *PCB*-manufactured prototype, has verified the *FW*-predicted radiation features over the operative band.

ACKNOWLEDGMENT

Andrea Massa would like to thank E. Vico for her never-ending inspiration, support, guidance, and help.

REFERENCES

[1] J. Hasch, E. Topak, R. Schnabel, T. Zwick, R. Weigel, and C. Waldschmidt, "Millimeter-wave technology for automotive radar sensors in the 77 GHz frequency band," *IEEE Trans. Microw. Theory Techn.*, vol. 60, no. 3, pp. 845–860, Mar. 2012.

[2] D. Kissinger, *Millimeter-Wave Receiver Concepts for 77 GHz Automotive Radar in Silicon-Germanium Technology*. New York, NY, USA: Springer-Verlag, 2012.

[6] The slight offset of the central frequency in the simulated S_{11} curve [Fig. 16(*b*) vs. Fig. 6] is caused by the modifications to the *PCB* layout in order to include the connector footprint and the vias [Fig. 16(*a*) vs. Fig. 5].

[3] M.-S. Kim and S.-S. Kim, "Design and fabrication of 77-GHz radar absorbing materials using frequency-selective surfaces for autonomous vehicles application," *IEEE Microw. Wireless Compon. Lett.*, vol. 29, no. 12, pp. 779–782, Dec. 2019.

[4] J. Overdevest, F. Jansen, F. Uysal, and A. Yarovoy, "Doppler influence on waveform orthogonality in 79 GHz MIMO phase-coded automotive radar," *IEEE Trans. Veh. Technol.*, vol. 69, no. 1, pp. 16–25, Jan. 2020.

[5] E. Klinefelter and J. A. Nanzer, "Automotive velocity sensing using millimeter-wave interferometric radar," *IEEE Trans. Microw. Theory Techn.*, vol. 69, no. 1, pp. 1096–1104, Jan. 2021.

[6] C.-H. Kuo, C.-C. Lin, and J.-S. Sun, "Modified microstrip Franklin array antenna for automotive short-range radar application in blind spot information system," *IEEE Antennas Wireless Propag. Lett.*, vol. 16, pp. 1731–1734, 2017.

[7] C.-A. Yu, E. S. Li, H. Jin, Y. Cao, G.-R. Su, W. Che, and K.-S. Chin, "24 GHz horizontally polarized automotive antenna arrays with wide fan beam and high gain," *IEEE Trans. Antennas Propag.*, vol. 67, no. 2, pp. 892–904, Feb. 2019.

[8] J. Xu, W. Hong, H. Zhang, G. Wang, Y. Yu, and Z. H. Jiang, "An array antenna for both long- and medium-range 77 GHz automotive radar applications," *IEEE Trans. Antennas Propag.*, vol. 65, no. 12, pp. 7207–7216, Dec. 2017.

[9] Y. Q. Guo, Y. M. Pan, and S. Y. Zheng, "Design of series-fed, single-layer, and wideband millimeter-wave microstrip arrays," *IEEE Trans. Antennas Propag.*, vol. 68, no. 10, pp. 7017–7026, Oct. 2020.

[10] M. Mosalanejad, I. Ocket, C. Soens, and G. A. E. Vandenbosch, "Wideband compact comb-line antenna array for 79 GHz automotive radar applications," *IEEE Antennas Wireless Propag. Lett.*, vol. 17, no. 9, pp. 1580–1583, Sep. 2018.

[11] S. Afoakwa and Y.-B. Jung, "Wideband microstrip comb-line linear array antenna using stubbed-element technique for high sidelobe suppression," *IEEE Trans. Antennas Propag.*, vol. 65, no. 10, pp. 5190–5199, Oct. 2017.

[12] Y. Hayashi, K. Sakakibara, M. Nanjo, S. Sugawa, N. Kikuma, and H. Hirayama, "Millimeter-wave microstrip comb-line antenna using reflection-canceling slit structure," *IEEE Trans. Antennas Propag.*, vol. 59, no. 2, pp. 398–406, Feb. 2011.

[13] L. Zhang, W. Zhang, and Y. P. Zhang, "Microstrip grid and comb array antennas," *IEEE Trans. Antennas Propag.*, vol. 59, no. 11, pp. 4077–4084, Nov. 2011.

[14] P. Hallbjorner, Z. He, S. Bruce, and S. Cheng, "Low-profile 77-GHz lens antenna with array feeder," *IEEE Antennas Wireless Propag. Lett.*, vol. 11, pp. 205–207, 2012.

[15] W. M. Abdel-Wahab, D. Busuioc, and S. Safavi-Naeini, "Millimeter-wave high radiation efficiency planar waveguide series-fed dielectric resonator antenna (DRA) array: Analysis, design, and measurements," *IEEE Trans. Antennas Propag.*, vol. 59, no. 8, pp. 2834–2843, Aug. 2011.

[16] E. Arnieri, F. Greco, L. Boccia, and G. Amendola, "A reduced size planar grid array antenna for automotive radar sensors," *IEEE Antennas Wireless Propag. Lett.*, vol. 17, no. 12, pp. 2389–2393, Dec. 2018.

[17] M. Mosalanejad, I. Ocket, C. Soens, and G. A. E. Vandenbosch, "Multilayer compact grid antenna array for 79 GHz automotive radar applications," *IEEE Antennas Wireless Propag. Lett.*, vol. 17, no. 9, pp. 1677–1681, Sep. 2018.

[18] M. Ettorre, R. Sauleau, L. Le Coq, and F. Bodereau, "Single-folded leaky-wave antennas for automotive radars at 77 GHz," *IEEE Antennas Wireless Propag. Lett.*, vol. 9, pp. 859–862, 2010.

[19] F. Bauer and W. Menzel, "A 79-GHz planar antenna array using ceramic-filled cavity resonators in LTCC," *IEEE Antennas Wireless Propag. Lett.*, vol. 12, pp. 910–913, 2013.

[20] S. Yoo, Y. Milyakh, H. Kim, C. Hong, and H. Choo, "Patch array antenna using a dual coupled feeding structure for 79 GHz automotive radar applications," *IEEE Antennas Wireless Propag. Lett.*, vol. 19, no. 4, pp. 676–679, Apr. 2020.

[21] X. Wang and A. Stelzer, "A 79-GHz LTCC patch array antenna using a laminated waveguide-based vertical parallel feed," *IEEE Antennas Wireless Propag. Lett.*, vol. 12, pp. 987–990, 2013.

[22] S. Cheng, H. Yousef, and H. Kratz, "79 GHz slot antennas based on substrate integrated waveguides (SIW) in a flexible printed circuit board," *IEEE Trans. Antennas Propag.*, vol. 57, no. 1, pp. 64–71, Jan. 2009.

[23] A. Dewantari, J. Kim, I. Scherbatko, and M.-H. Ka, "A sidelobe level reduction method for mm-wave substrate integrated waveguide slot array antenna," *IEEE Antennas Wireless Propag. Lett.*, vol. 18, no. 8, pp. 1557–1561, Aug. 2019.

[24] Y. Yu, W. Hong, H. Zhang, J. Xu, and Z. H. Jiang, "Optimization and implementation of SIW slot array for both medium- and long-range 77 GHz automotive radar application," *IEEE Trans. Antennas Propag.*, vol. 66, no. 7, pp. 3769–3774, Jul. 2018.

[25] M. S. Abdallah, Y. Wang, W. M. Abdel-Wahab, and S. Safavi-Naeini, "Design and optimization of SIW center-fed series rectangular dielectric resonator antenna array with 45° linear polarization," *IEEE Trans. Antennas Propag.*, vol. 66, no. 1, pp. 23–31, Jan. 2018.

[26] J. Xu, Z. N. Chen, and X. Qing, "CPW center-fed single-layer SIW slot antenna array for automotive radars," *IEEE Trans. Antennas Propag.*, vol. 62, no. 9, pp. 4528–4536, Sep. 2014.

[27] R. Chopra and G. Kumar, "Series-fed binomial microstrip arrays for extremely low sidelobe level," *IEEE Trans. Antennas Propag.*, vol. 67, no. 6, pp. 4275–4279, Jun. 2019.

[28] N. Boskovic, B. Jokanovic, M. Radovanovic, and N. S. Doncov, "Novel Ku-band series-fed patch antenna array with enhanced impedance and radiation bandwidth," *IEEE Trans. Antennas Propag.*, vol. 66, no. 12, pp. 7041–7048, Dec. 2018.

[29] H. Yi, L. Li, J. Han, and Y. Shi, "Traveling-wave series-fed patch array antenna using novel reflection-canceling elements for flexible beam," *IEEE Access*, vol. 7, pp. 111466–111476, 2019.

[30] Z. Ahmed, M. John, P. Mcevoy, and M. J. Ammann, "Investigation of frequency scanning printed Bruce array antenna," *IEEE Access*, vol. 8, pp. 189003–189012, 2020.

[31] S. David Joseph and E. A. Ball, "Series-fed millimeter-wave antenna array based on microstrip line structure," *IEEE Open J. Antennas Propag.*, vol. 4, pp. 254–261, 2023.

[32] H. Yi, Z. Wang, D. Xia, H. Liu, and L. Li, "Periodic asymmetric trapezoidal perturbation microstrip antenna for millimeter-wave automotive radar sensors," *IEEE Trans. Antennas Propag.*, vol. 71, no. 2, pp. 1369–1377, Feb. 2023.

[33] M. Salucci, F. Robol, N. Anselmi, M. A. Hannan, P. Rocca, G. Oliveri, M. Donelli, and A. Massa, "S-band spline-shaped aperture-stacked patch antenna for air traffic control applications," *IEEE Trans. Antennas Propag.*, vol. 66, no. 8, pp. 4292–4297, Aug. 2018.

[34] L. Lizzi, F. Viani, R. Azaro, and A. Massa, "A PSO-driven spline-based shaping approach for ultrawideband (UWB) antenna synthesis," *IEEE Trans. Antennas Propag.*, vol. 56, no. 8, pp. 2613–2621, Aug. 2008.

[35] G. Oliveri, G. Gottardi, F. Robol, A. Polo, L. Poli, M. Salucci, M. Chuan, C. Massagrande, P. Vinetti, M. Mattivi, R. Lombardi, and A. Massa, "Codesign of unconventional array architectures and antenna elements for 5G base stations," *IEEE Trans. Antennas Propag.*, vol. 65, no. 12, pp. 6752–6767, Dec. 2017.

[36] M. Salucci, G. Oliveri, M. A. Hannan, and A. Massa, "System-by-Design paradigm-based synthesis of complex systems: The case of spline-contoured 3D radomes," *IEEE Antennas Propag. Mag.*, vol. 64, no. 1, pp. 72–83, Feb. 2022.

[37] A. Massa and M. Salucci, "On the design of complex EM devices and systems through the system-by-design paradigm: A framework for dealing with the computational complexity," *IEEE Trans. Antennas Propag.*, vol. 70, no. 2, pp. 1328–1343, Feb. 2022.

[38] P. Rosatti, M. Salucci, L. Poli, and A. Massa, "Multiobjective system-by-design for mm-wave automotive radar antennas," *IEEE Trans. Antennas Propag.*, vol. 71, no. 4, pp. 2958–2973, Apr. 2023.

[39] S. Goudos, *Emerging Evolutionary Algorithms for Antennas and Wireless Communications*. Stevenage, U.K.: SciTech, 2021.

[40] S. K. Goudos, C. Kalialakis, and R. Mittra, "Evolutionary algorithms applied to antennas and propagation: A review of state of the art," *Int. J. Antennas Propag.*, vol. 2016, pp. 1–12, 2016.

[41] P. Rocca, M. Benedetti, M. Donelli, D. Franceschini, and A. Massa, "Evolutionary optimization as applied to inverse scattering problems," *Inverse Problems*, vol. 25, no. 12, Dec. 2009, Art. no. 123003.

[42] A. Massa, G. Oliveri, M. Salucci, N. Anselmi, and P. Rocca, "Learning-by-examples techniques as applied to electromagnetics," *J. Electromagn. Waves Appl.*, vol. 32, no. 4, pp. 516–541, Mar. 2018.

[43] K. Tan, T. Yin, H. Ruan, S. Balon, and X. Chen, "Learning approach to FMCW radar target classification with feature extraction from wave physics," *IEEE Trans. Antennas Propag.*, vol. 70, no. 8, pp. 6287–6299, Aug. 2022.

[44] W. A. Ahmad, M. Kucharski, A. Ergintav, H. J. Ng, and D. Kissinger, "A planar differential wide fan-beam antenna array architecture: Modular high-gain array for 79-GHz multiple-input, multiple-output radar applications," *IEEE Antennas Propag. Mag.*, vol. 63, no. 4, pp. 21–32, Aug. 2021.

[45] *ANSYS Electromagnetics Suite—HFSS*, ANSYS, Canonsburg, PA, USA, 2021.

MARCO SALUCCI (Senior Member, IEEE) received the M.S. degree in telecommunication engineering from the University of Trento, Italy, in 2011, and the Ph.D. degree from the International Doctoral School in Information and Communication Technology of Trento, in 2014. He was a Postdoctoral Researcher with CentraleSupélec, Paris, France, and a Postdoctoral Researcher with Commissariat à l'Énergie Atomique et aux Énergies Alternatives (CEA), France. He is currently a tenure track Associate Professor with the Department of Civil, Environmental, and Mechanical Engineering (DICAM), University of Trento, and a Research Fellow of the ELEDIA Research Center. In 2023, he co-edited the book *Applications of Deep Learning in Electromagnetics—Teaching Maxwell's Equations to Machines* (IET). His research interests include inverse scattering, biomedical and GPR microwave imaging techniques, antenna synthesis, and computational electromagnetics, with a focus on system-by-design methodologies integrating optimization techniques and artificial intelligence for real-world applications. He is a member of the IEEE Antennas and Propagation Society. He was a member of the COST Action TU1208 "Civil Engineering Applications of Ground Penetrating Radar." He is also an Associate Editor of *Communications* and Memberships of IEEE TRANSACTIONS ON ANTENNAS AND PROPAGATION. Moreover, he serves as an Associate Editor for IEEE TRANSACTIONS ON ANTENNAS AND PROPAGATION, the IEEE OPEN JOURNAL OF ANTENNAS AND PROPAGATION, and the *International Journal of Microwave and Wireless Technologies*. Furthermore, he serves as a Reviewer for different international journals, including IEEE TRANSACTIONS ON ANTENNAS AND PROPAGATION, IEEE TRANSACTIONS ON MICROWAVE THEORY AND TECHNIQUES, IEEE TRANSACTIONS ON GEOSCIENCE AND REMOTE SENSING, and the IEEE JOURNAL ON MULTISCALE AND MULTIPHYSICS COMPUTATIONAL TECHNIQUES.

LORENZO POLI (Senior Member, IEEE) received the M.S. degree in telecommunication engineering from the University of Trento, Italy, in 2008, and the Ph.D. degree from the International Doctoral School in Information and Communication Technology, in 2012. He is currently an Assistant Professor with the Department of Civil, Environmental, and Mechanical Engineering (DICAM), University of Trento, and a Research Fellow of the ELEDIA Research Center. He is the author/coauthor of more than 60 journals and 90 conference papers. He was a Visiting Researcher with Laboratoire des Signaux et Systèmes (L2S@Supélec), France, in 2015, and a Visiting Professor with the University of Paris Sud, France, in 2016. He has been a member of the IEEE Antennas and Propagation Society, since 2010, when he was a recipient of the IEEE Antennas and Propagation Society Doctoral Research Award. He serves as a Reviewer for several international journals, including IEEE TRANSACTIONS ON ANTENNAS AND PROPAGATION, IEEE ANTENNAS AND WIRELESS PROPAGATION LETTERS, and *IET Microwaves, Antennas & Propagation*. His research interests include the solution of antenna design and unconventional array synthesis problems and electromagnetic inverse scattering problems.

PAOLO ROCCA (Fellow, IEEE) received the M.S. degree (summa cum laude) in telecommunications engineering and the Ph.D. degree in information and communication technologies from the University of Trento, Italy, in 2005 and 2008, respectively. He is currently an Associate Professor with the Department of Civil, Environmental, and Mechanical Engineering, University of Trento; the Huashan Scholar Chair Professor with Xidian University, Xi'an, China; and a member of the ELEDIA Research Center. Moreover, he is a member of the Big Data and AI Working Group for the Committee on Engineering for Innovative Technologies (CEIT) of the World Federation of Engineering Organizations (WFEO). He received the National Scientific Qualification for the position of a Full Professor in Italy and France, in April 2017 and January 2020, respectively. He has been a Visiting Ph.D. Student with The Pennsylvania State University, USA, and the Mediterranea University of Reggio Calabria, Italy; and a Visiting Researcher with Laboratoire des Signaux et Systèmes (L2S@ Supélec), France, in 2012 and 2013. Moreover, he has been an invited Professor with the University of Paris Sud, France, in 2015, and the University of Rennes 1, France, in 2017. He is the author/coauthor of two book chapters, 165 journal articles, and more than 290 conference papers. His main research interests include the framework of artificial intelligence techniques as applied to electromagnetics, antenna array synthesis and analysis, electromagnetic inverse scattering, and quantum computing for electromagnetic engineering. He has been awarded from the IEEE Geoscience and Remote Sensing Society and the Italy Section with the Best Ph.D. Thesis Award IEEE-GRS Central Italy Chapter. He served as an Associate Editor for the IEEE ANTENNAS AND WIRELESS PROPAGATION LETTERS, from 2011 to 2016, and the *Microwave and Optical Technology Letters*, from 2019 to 2020. He has been serving as an Associate Editor for *IEEE Antennas and Propagation Magazine*, since 2020, and *Engineering*, since 2020.

CLAUDIO MASSAGRANDE (Member, IEEE) received the master's degree in electronic engineering (telecommunications) from Politecnico di Milano, Milan, Italy, in 1996. He is currently a Principal Antenna Engineer with the Huawei Milan Research Center (MiRC), Milan. He has almost 25 years of experience in the telecom industry as a Microwave and Antenna Designer for Andrew (now Commscope), Siemens (then Nokia Siemens Networks), and Huawei Technologies. During his carrier, he designed, developed, and tested front ends of several families of microwave radios gaining considerable experience in microwave assembly technologies, such as chip and wire and die attach. His expertise ranges from radio frequency design for microwave PTP radio links for the mobile network backhaul to radio link integration to advanced antenna systems design. His current research interest includes advanced antenna systems for mm-wave 5G access.

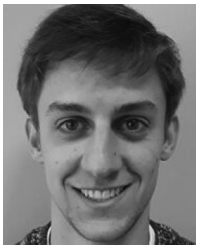

PIETRO ROSATTI received the B.Sc. degree in electronics and telecommunications engineering and the M.Sc. degree in information and communication engineering from the University of Trento, Trento, Italy, in 2017 and 2020, respectively, where he is currently pursuing the Ph.D. degree in information and communication technology with the International Doctoral School. He is also a Senior Researcher with the ELEDIA Research Center, University of Trento. His research interests include the design and analysis of wide-angle phased array antennas for modern applications, such as automotive radars and 5G communications.

MOHAMMAD ABDUL HANNAN received the B.Sc. degree in electronics and telecommunication engineering (ETE) from Daffodil International University, Bangladesh, in 2010, the master's degree in telecommunication engineering from the University of Trento, Italy, in 2015, and the Ph.D. degree from the International Doctoral School in Information and Communication Technology, Trento, Italy, in 2020. He is currently an Assistant Professor with the Department of Electrical Electronic and Computer Engineering, University of Catania, Italy, and a Senior Researcher with the ELEDIA Research Center. His research interests include electromagnetic direct and inverse scattering and antenna system synthesis for sensing and communications.

MIRKO FACCHINELLI received the B.Sc. degree in communication and information engineering and the M.Sc. degree in information and communication engineering from the University of Trento, Trento, Italy, in 2021 and 2023, respectively. He is currently an ETRP-Advanced with the ELEDIA Research Center. His research interest includes the optimization techniques for the design of simplified antenna arrays.

ANDREA MASSA (Fellow, IEEE) received the Laurea (M.S.) degree in electronic engineering and the Ph.D. degree in EECS from the University of Genoa, Genoa, Italy, in 1992 and 1996, respectively. He is currently a Full Professor in electromagnetic fields with the University of Trento, where he also teaches electromagnetic fields, inverse scattering techniques, antennas and wireless communications, wireless services and devices, and optimization techniques. He is also the Director of the Network of Federated Laboratories, ''ELEDIA Research Center'' (www.eledia.org) located in Brunei, China, Czech, France, Greece, Italy, Japan, Perú, and Tunisia, with more than 150 researchers. Moreover, he is also the Holder of a Chang-Jiang Chair Professorship with UESTC, Chengdu, China; a Visiting Research Professor with the University of Illinois at Chicago, Chicago, USA; a Visiting Professor with Tsinghua University, Beijing, China; a Visiting Professor with Tel Aviv University, Tel Aviv, Israel; and a Professor with CentraleSupélec, Paris, France. He has been the Holder of the Senior DIGITEO Chair, L2S-CentraleSupélec, and CEA LIST, Saclay, France; the UC3M-Santander Chair of Excellence with Universidad Carlos III de Madrid, Spain; an Adjunct Professor with Penn State University, USA; a Guest Professor with UESTC, China; and a Visiting Professor with the Missouri University of Science and Technology, USA, Nagasaki University, Japan, the University of Paris Sud, France, Kumamoto University, Japan, and the National University of Singapore, Singapore. He has published more than 900 scientific publications among which more than 350 on international journals [more than 15 000 citations H-index = 65 (Scopus); more than 12 000 citations H-index = 59 (ISI-WoS); and more than 23 000 citations H-index = 89 (Google Scholar)] and more than 550 in international conferences, where he presented more than 200 invited contributions (more than 40 invited keynote speaker) (www.eledia.org/publications). He has organized more than 100 scientific sessions in international conferences and has participated to several technological projects in the national and international framework with both national agencies and companies (18 international prj, > 5 MEu; eight national prj, > 5 MEu; ten local prj, > 2 MEu; 63 industrial prj, > 10 MEu; and six university prj, > 300 KEu). His research interests include inverse problems, analysis synthesis of antenna systems and large arrays, radar systems synthesis and signal processing, cross-layer optimization and planning of wireless RF systems, semantic wireless technologies, system-by-design and material-by-design (metamaterials and reconfigurable-materials), and theory applications of optimization techniques to engineering problems (tele-communications, medicine, and biology). He is also a fellow of IET and Electromagnetic Academy. He is a member of the Editorial Board of the *Journal of Electromagnetic Waves and Applications*, a permanent member of the ''PIERS Technical Committee'' and of the ''EuMW Technical Committee,'' and a ESoA Member. He has been appointed in the Scientific Board of ''Societá Italiana di Elettromagnetismo (SIEm)'' and elected in the Scientific Board of the Interuniversity National Center for Telecommunications (CNIT). He has been appointed, in 2011, by the National Agency for the Evaluation of the University System and National Research (ANVUR) as a member of the Recognized Expert Evaluation Group (Area nine, ''Industrial and Information Engineering'') for the evaluation of the researches with the Italian University and Research Center, from 2004 to 2010. Furthermore, he has been elected as the Italian Member of the Management Committee of the COST Action TU1208 ''Civil Engineering Applications of Ground Penetrating Radar.'' He has been appointed IEEE APS Distinguished Lecturer, from 2016 to 2018, and served as an Associate Editor for IEEE TRANSACTIONS ON ANTENNAS AND PROPAGATION,'' from 2011 to 2014. He serves as an Associate Editor for the *International Journal of Microwave and Wireless Technologies*.''

Open Access funding provided by 'Università degli Studi di Trento' within the CRUI CARE Agreement